applied sciences

MDPI

Article

An Improved Cyclic Modulation Spectral Analysis Based on the CWT and Its Application on Broken Rotor Bar Fault Diagnosis for Induction Motors

Dong Zhen [1], Zuolu Wang [1], Haiyang Li [2], Hao Zhang [1,*], Jie Yang [1,*] and Fengshou Gu [2]

[1] Tianjin Key Laboratory of Power Transmission and Safety Technology for New Energy Vehicles, School of Mechanical Engineering, Hebei University of Technology, Tianjin 300401, China; d.zhen@hebut.edu.cn (D.Z.); zl_wang66@163.com (Z.W.)

[2] Centre for Efficiency and Performance Engineering, University of Huddersfield, Huddersfiled HD1 3DH, UK; Haiyang.Li@hud.ac.uk (H.L.); f.gu@hud.ac.uk (F.G.)

* Correspondence: zhanghao@hebut.edu.cn (H.Z.); 2010002@hebut.edu.cn (J.Y.); Tel.: +86-22-2658-2598 (H.Z. & J.Y.)

Received: 6 August 2019; Accepted: 12 September 2019; Published: 17 September 2019

Abstract: Induction motors (IMs) are widely used in many manufacturing processes and industrial applications. The harsh work environment, long-time enduring, and overloads mean that it is subjected to broken rotor bar (BRB) faults. The vibration signal of IMs with BRB faults consists of the reliable modulation information used for fault diagnosis. Cyclostationary analysis has been found to be effective in identifying and extracting fault feature. The estimators of cyclic modulation spectrum (CMS) and fast spectral correlation (FSC) based on the short-time fourier transform (STFT) have higher cyclic frequency resolution, which has proven efficient in demodulating second order cyclostationary (CS2) signals. However, these two estimators have limitations of processing the maximum cyclic frequency α_{max} that is smaller than $Fs/2$ (Fs is the sampling frequency) according to Nyquist's Theorem. In addition, they have lower carrier frequency resolution due to the fixed window size used in STFT. In order to resolve the initial shortcomings of the CMS and FSC methods, in this paper, we extended the analysis of CMS algorithm based on the continuous wavelet transform (CWT), which enlarged the maximum cyclic frequency range to $Fs/2$ and provides higher carrier frequency resolution because the CWT has the advantage of multi-resolution analysis. The reliability and applicability of the proposed method for fault components localization were validated by CS2 simulation signals. Compared to CMS and FSC methods, the proposed approach shows better performance by analyzing vibration signals between healthy motor and faulty motor with one BRB fault under 0%, 20%, 40%, and 80% load conditions.

Keywords: induction motor; broken rotor bar; cyclic modulation spectral; continuous wavelet transform

1. Introduction

Induction motor (IM) is one of the most popular pieces of mechanical equipment and plays an important part in industrial applications. However, the harsh operation environment and gradual wearing make it be liable to failure. Broken rotor bar (BRB) in IMs represents 8–9% of IM faults but they bring serious breakdown and lead to loss of productivity [1]. This needs to be solved, otherwise it can cause multiple BRB faults, mechanical eccentricity, and thermal stress because of localized heating. The detection of this type of fault has been a key issue of studies which aims to develop more advanced techniques to minimize the breakdown and maintenance cost of IMs.

Several sensing techniques have been researched in the field of BRB fault diagnosis. For example, motor current signature analysis (MCSA) [2–17] is the mainstream technique, and the motor vibration

signature analysis (MVSA) [18–32] technique is commonly used for diagnosing the presence of BRB failures. However, the sound measurement [32], temperature measurement [33], and magnetic field analysis [34] have been used less due to the inference of external factors. Among them, vibration signature analysis has become an effective tool in the field of condition monitoring and fault diagnosis of rotating machinery [35]. Also, the vibration signature of the motor under different loads is easy to measure and can provide rich dynamic information reflecting BRB health status. Some authors proposed that vibration signal can be the fault symptom as well as electric signal [36,37].

Like other rotating machinery, the vibration signals of IMs with BRB faults generally include modulation components that are the culprit of BRB failures and have close connection with fault diagnosis. This type of modulation signal is non-stationary, thus useful methods need to effectively extract the modulation components reflecting the BRB faults. In recent years, many advanced techniques for BRB fault detection in IMs have been developed based on the vibration signature analysis and obtained good diagnostic results. For instance, the authors proposed an approach based on the use of frequency sliding and wavelet (WT) analysis to isolate the contribution of the BRB fault characteristics issued from vibration signals [25]. Vincent et al. [27] presented the analysis of BRB faults in a three-phase squirrel cage IM using an artificial intelligence method. Morales-Perez et al. [28] applied the sparse representation methodology to the detection of BRB fault based on the vibration signals from IMs. Also, Martinez, et al. [29] presented the development of analytical equations for vibration detection under successive broken bars and showed the relation between the number of broken bars and the vibration amplitudes. In addition, the orthogonal matching pursuit algorithm (OMP) in [30] was used for the decomposition of signals, which demonstrated that the detection accuracy is higher. Also, researchers in [31] developed a technique based on the vibration magnitudes of electromagnetic force for the rotor bar breakages detection in a squirrel-cage IM. Furthermore, Delgado-Arredondo et al. [32] used the complete ensemble empirical mode decomposition (CEEMD) for the fault diagnosis of BRB faults based on vibration analysis, which solved the drawback of ensemble empirical mode decomposition (EEMD) and the empirical mode decomposition (EMD) in signal processing.

The above vibration detection methods are based on the non-stationary level for the BRB fault diagnosis. Meanwhile, cyclostationary analysis has been proven to be effective for the analysis of second order cyclostationary (CS2) signals based on cyclostationary level. Cyclostationary analysis is a kind of special "time–frequency" demodulation tool, where the time axis represents the cyclic or modulation frequency domain, and the frequency axis denotes the carrier frequency domain. Moreover, CS2 signal is a type of special non-stationary signal that includes periodic modulation contents related to mechanical failures [38]. For example, the Fourier transform (FT) is effective in processing first order cyclostationary (CS1) signals, and it has been proven theoretically and practically not applicable to the identification of CS2 contents [39]. The BRB fault vibration signals issued from IMs are CS2 signals, which can be effectively processed via cyclostationary analysis methods. The cyclic modulation spectral (CMS) and fast spectral correlation (FSC) based on the short-time Fourier transform (STFT) proposed by Antoni in 2007 [40] and 2017 [41], respectively, are two computationally efficient cyclostationary analysis approaches, and their effectiveness and high efficiency were validated on bearing faults signals. Besides, they have the advantages of high cycle frequency resolution and the resolution is Fs/L (Fs denotes the sampling frequency and L is sampling points). On the one hand, although CMS can be performed efficiently, it still has the limitation that the maximum cyclic frequency α_{max} that can be analyzed is not more than Δf ($\Delta f = Fs/Nw$ and Nw is the window length used in STFT). Hence, the introduce of FSC compensates the deficiency of CMS, and it not only enlarges the range α_{max} to $Fs/2R$ (R is the step size of window used in STFT), but also still guarantees high computational efficiency. However, the existence of R limits the range of α_{max} for FSC. Meanwhile the α_{max} can be normally extended to $Fs/2$ by setting the R to 1, which makes the analysis of FSC method increase the computational cost and the redundancy of the signal. At the same time, these two methods cannot provide a satisfactory carrier frequency resolution because the STFT has a well-known limitation on time–frequency resolution, mainly due to the use of a fixed window size. However, the STFT can only

offer the time-frequency information with lower precision, and this precision is determined by just the window size. In the application of STFT, the time domain and frequency domain resolution cannot be optimized simultaneously. However, it requires a more flexible method, which can adaptively change the window size to receive more accurate time or frequency [42].

In the case of good time–frequency localization performance of wavelet transform, a new approach was proposed in this paper that optimized the CMS algorithm based on the use of the continuous wavelet transform (CWT) to overcome the deficiencies from simple CMS and FSC and provide more accurate analysis results. The CWT adopts multi-scale analysis by analyzing lower frequencies with larger window size and analyzing higher frequencies with smaller window size. This makes CWT adaptively choose finer frequency resolution and coarser time resolution when processing lower frequencies, while choose coarse frequency resolution and finer time resolution at higher frequencies. Positioning the local features of the sample can improve recognition accuracy [43]. The CWT is a useful method to characterize local time–frequency characteristic of non-stationary signals [44]. As a result, the proposed method combining CMS and CWT (CMS-CWT) approaches has the ability to enlarge the range of detectable modulation frequencies α_{max} to $Fs/2$ and make sure the cyclic frequency resolution is still Fs/L. Meanwhile, it can receive higher carrier frequency resolution than CMS and FSC based on the STFT method. In order to verify the effectiveness and performance, the proposed approach is validated using CS2 simulation signals and vibration signals collected from healthy IM and faulty motor with one BRB fault under various load conditions.

The rest of the paper is organized as follows: the brief description of CMS-CWT method is presented in Section 2. Subsequently, the Section 3 shows the simulation results of synthetic signals. The effectiveness is validated through experimental setup in Section 4 and finally the conclusion drawn from this work is given in Section 5.

2. The Cyclic Modulation Spectral Based on Continuous Wavelet Transform

The CWT is widely used in signal processing as an effective time–frequency analysis tool. It is able to construct a time–frequency representation of a signal that shows better time and frequency localization. CWT analysis also allows for choosing a longer time interval when a more precise low-frequency feature is needed, and shorter ones when high-frequency information is desired. It is operated by breaking up a signal into shifted and scaled versions of the mother wavelet, so that the local features can be described better with wavelets that are concentrated on a localized region [45]. The CWT of a signal $x(t)$ is defined as a convolution integral of $x(t)$ with scaled versions of a mother wavelet function $\Psi\tau, c(t)$ and is given by Equation (1):

$$W_x(\tau, c) = \frac{1}{\sqrt{c}} \int_{-\infty}^{+\infty} x(t) \Psi^*(\frac{t-\tau}{c}) dt \tag{1}$$

where $\Psi^*(t)$ is the complex conjugate of $\Psi(t)$, c is the scale parameter for changing the oscillating frequency, and τ is the translation parameter. Because the CWT is performed through convolution between wavelet function and original signal, the $\tau = 0, 1, 2... L-1$ (L denotes the length of original signal). There are a number of different wavelet functions that can be utilized for CWT analysis. In this work, the Coif4 wavelet is determined as the mother wavelet due to its similarity to a BRB fault component that is a fault characteristic in an IMs. Theoretically, the actual signal frequency corresponding to the scale parameter c is $f = Fc \cdot Fs/c$ (Fc is the wavelet center frequency, and Fs is the sampling frequency). According to the equivalence between f and c, Equation (1) can be turned into Equation (2) as follows:

$$W_x(\tau, f) = \frac{1}{\sqrt{c}} \int_{-\infty}^{+\infty} x(t) \Psi^*(\frac{t-\tau}{c}) dt \tag{2}$$

Then, it is noted that $\left|W_x(\tau, f)\right|^2$ can reflect the intensity as well as the distribution of signal energy, which is an important distinction between fault components and noise components. At last,

the CMS-CWT algorithm can be efficiently computed as the discrete Fourier transform (DFT), which causes time variable τ to be converted into cyclic frequency variable α.

$$S_x^{CMS-CWT}(\alpha, f) = \frac{1}{L \cdot Fs} \sum_{\tau=0}^{L-1} \left| W_x(\tau, f) \right|^2 e^{-j2\pi\tau \frac{\alpha}{Fs}} \quad (3)$$

In the case of the CMS and FSC based on STFT, the number used for DFT is the total number of *Nw*-long window shifted by *R* samples in a *L*-long signal. In contrast, the proposed CMS-CWT method uses the *L*-length signal to do DFT every time. This is the reason why CMS-CWT method can flexibly handle the signal with the maximum cycle frequency associated with the faults in the range of 0–*Fs*/2. Theoretical analysis shows that the proposed method can provide the same cyclic frequency resolution as CMS and FSC. All in all, this method can provide a larger cycle frequency analysis range and more accurate carrier frequency resolution than CMS and FSC. The flowchart of the proposed method based on CMS-CWT is shown in Figure 1.

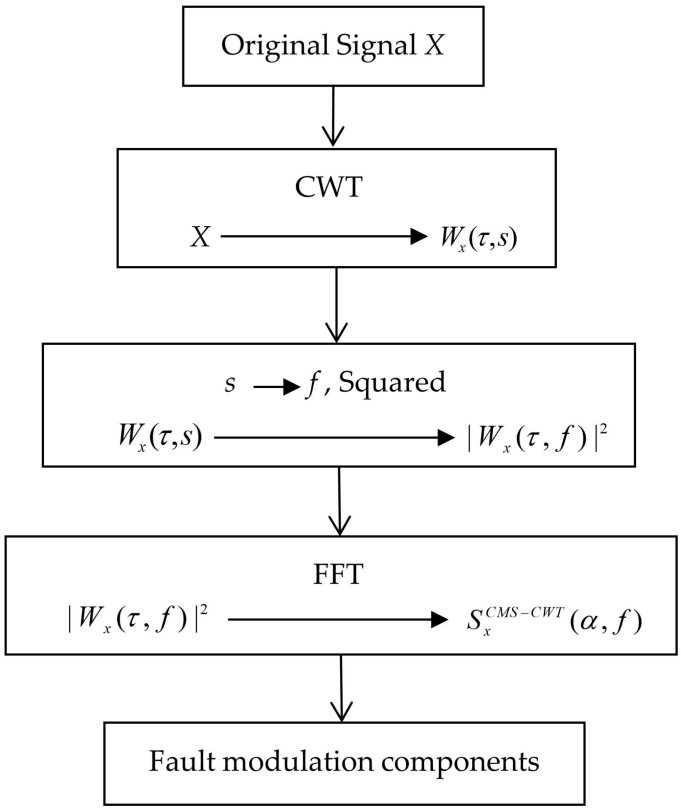

Figure 1. The flowchart of the proposed method.

3. Simulation Study

As shown in Equation (4), a synthetic fault signal equivalent to the BRB fault signal that is also a kind of CS2 signal is established to verify the performance of the proposed method. Where α is the main cyclic frequency caused by BRB faults and f_r denotes the carrier frequency of IMs. When the BRB fault occurs, the main cyclic frequency α will modulate on the rotation frequency f_r or its harmonics. Where A_1 and A_2 represents the amplitudes of α and f_r, and the simulated signal was corrupted by Gaussian white noise $n(t)$ with the signal-to-noise ratio (SNR) of −2 dB. The simulation analysis was done by processing the signal expressed in Equation (4) with the amplitudes $A_1 = A_2 = 1$ and two different sets of cyclic frequencies and carrier frequencies. The frequency settings were $\alpha_1 = 4$ Hz, $f_{r1} = 40$ Hz and $\alpha_2 = 100$ Hz, $f_{r2} = 400$ Hz. In addition, the sampling frequency *Fs* and sampling points

L of simulation signal was setup as 1000 Hz and 10^5, respectively. It needs to be noted that all data processing is performed on a computer with an i5-7400 CPU processor 3.00 GHz.

$$x_{BRB}(t) = (1 + A_1 \cdot \sin(2 \cdot \pi \cdot \alpha \cdot t)) \cdot A_2 \cdot \sin(2 \cdot \pi \cdot f_r \cdot t) + n(t) \quad (4)$$

Firstly, the advantage of larger cyclic frequency range of CMS-CWT method will be verified. In the processing of the CMS and FSC methods based on STFT, a Hamming window of length $Nw = 2^7$ was used for STFT calculation and the step size R is set to 25% of the window length (R = 32). The total number of windows shifted by R samples in a L-long signal is K = 3122. Table 1 presents the cyclic frequency resolution and the maximum cycle frequency values that can be analyzed through three approaches based on the simulated signals.

Table 1. Parameters setting.

Parameters	CMS	FSC	CMS-CWT
$\Delta\alpha$	Fs/L	Fs/L	Fs/L
Value	0.01 Hz	0.01 Hz	0.01 Hz
α_{max}	Fs/Nw	$Fs/2R$	$Fs/2$
Value	7.8125 Hz	15.625 Hz	500 Hz

CMS: cyclic modulation spectrum; FSC: fast spectral correlation; CMS-CWT: cyclic modulation spectrum-continuous wavelet transform.

As shown in Figure 2, the CMS method can only analyze the signal with the cyclic frequency in the range of 0–Fs/Nw. When the cycle frequency to be analyzed is greater than 7.8125, the signal begins to drift downward, which greatly limits the signal analysis ability of the CMS algorithm. Although the FSC method extends the analysis range to $Fs/2R$ as illustrated in Figure 3, the cyclic frequencies of 15.625–500 Hz cannot be analyzed and processed effectively, which significantly limits the application of the FSC method in condition monitoring and fault diagnosis fields. According to the analysis results presented in Figure 4, the proposed CMS-CWT approach received a better analysis in the range of 0–500 Hz. Furthermore, the FSC can enlarge the cyclic frequency range to 500 Hz by setting R to 1, but it can be seen from Figure 5 the signal generates drift, which increased both signal redundancy and computational cost due to excessive signal overlap in the calculation of STFT. Moreover, the FSC took 109.053 s to get analysis result as shown in Figure 5 compared to 3.5920 s utilized by CMS-CWT to process the same data as shown in Figure 4. In short, the proposed CMS-CWT approach can provide larger analysis range of cyclic frequency and more accurate diagnosis results than the CMS and FSC in the cyclic frequency axis.

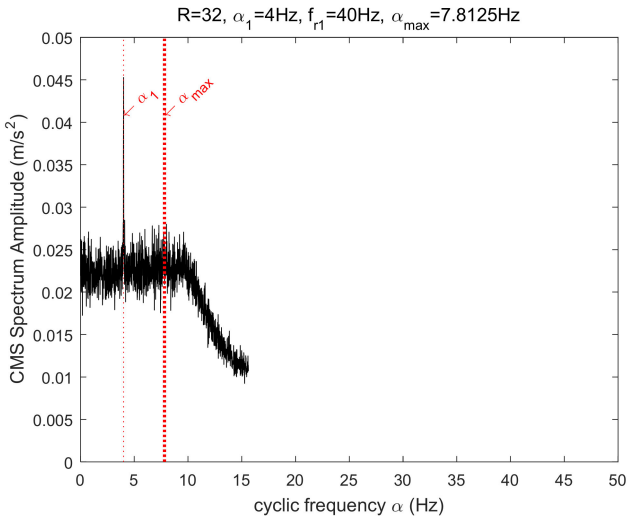

Figure 2. Vibration spectrum analyzed by cyclic modulation spectrum (CMS) with R = 32.

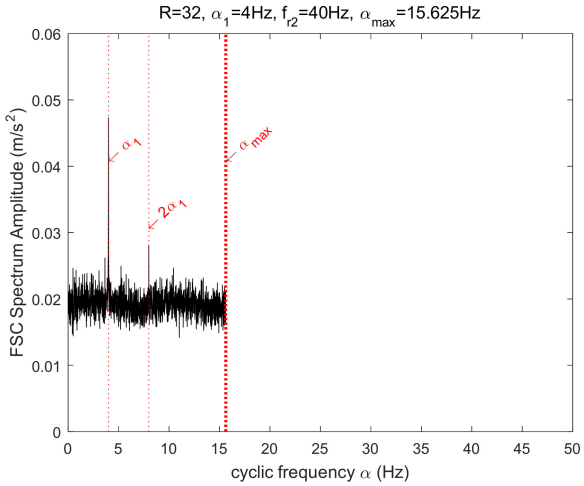

Figure 3. Vibration spectrum analysed by fast spectral correlation (FSC) with R = 32.

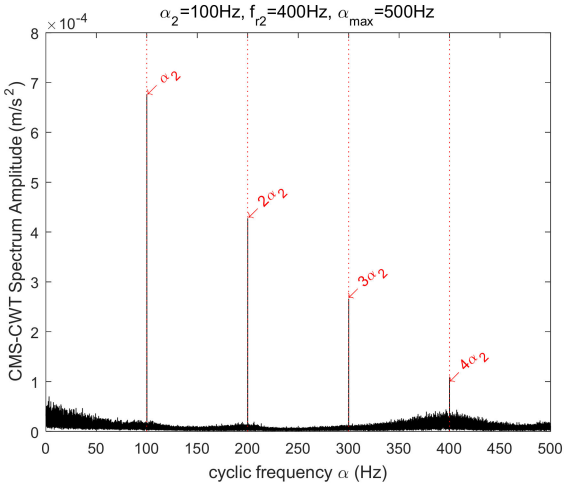

Figure 4. Vibration spectrum analyzed by cyclic modulation spectral-continuous wavelet transform (CMS-CWT).

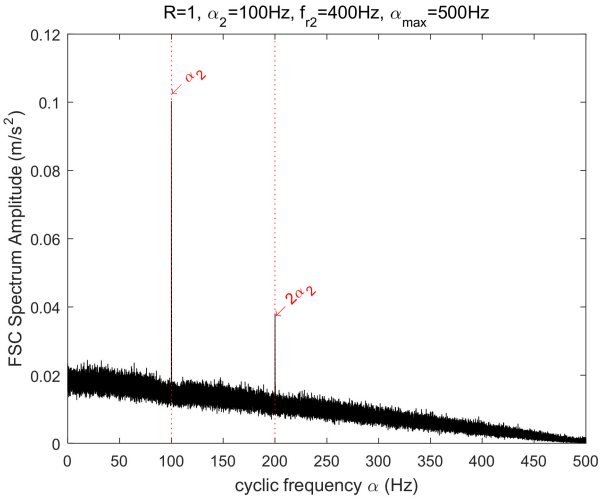

Figure 5. Vibration spectrum analysed by FSC with R = 1.

Moreover, the strength of higher carrier frequency resolution of CMS-CWT algorithm was verified. According to the Equation (4), two simulation signals with sampling rates of 1000 Hz and 10,000 Hz

were established and processed by three methods as shown in Table 2, and other settings are the same as the simulation analysis above.

Table 2. Parameters settings used in simulated signal.

Group	*Fs*	*L*	*α*	*f*	Window	*Nw*	*R*
First group	1000 Hz	10^5	4 Hz	40 Hz	Hamming	2^7	32
Second group	10,000 Hz	10^5	4 Hz	40 Hz	Hamming	2^7	32

The STFT shows a kind of compromise between the time resolution and frequency resolution of a signal. According to the analysis results as shown in Figures 6 and 7, the CMS and FSC have lower carrier frequency resolution than CMS-CWT. As the increasing of sampling frequency, the CMS and FSC cannot distinguish the carrier frequency components modulated by the cyclic frequency at all due to the fixed window length used in the STFT. However, the proposed CMS-CWT method can obtain a higher carrier frequency resolution by adjusting the scale parameter, which enables it to accurately identify the carrier frequency components modulated by the fault frequency. Simulation results shown the local information can be displayed better with CMS-CWT method because of its ability to localize both cyclic frequency and carrier frequency in a more precise way.

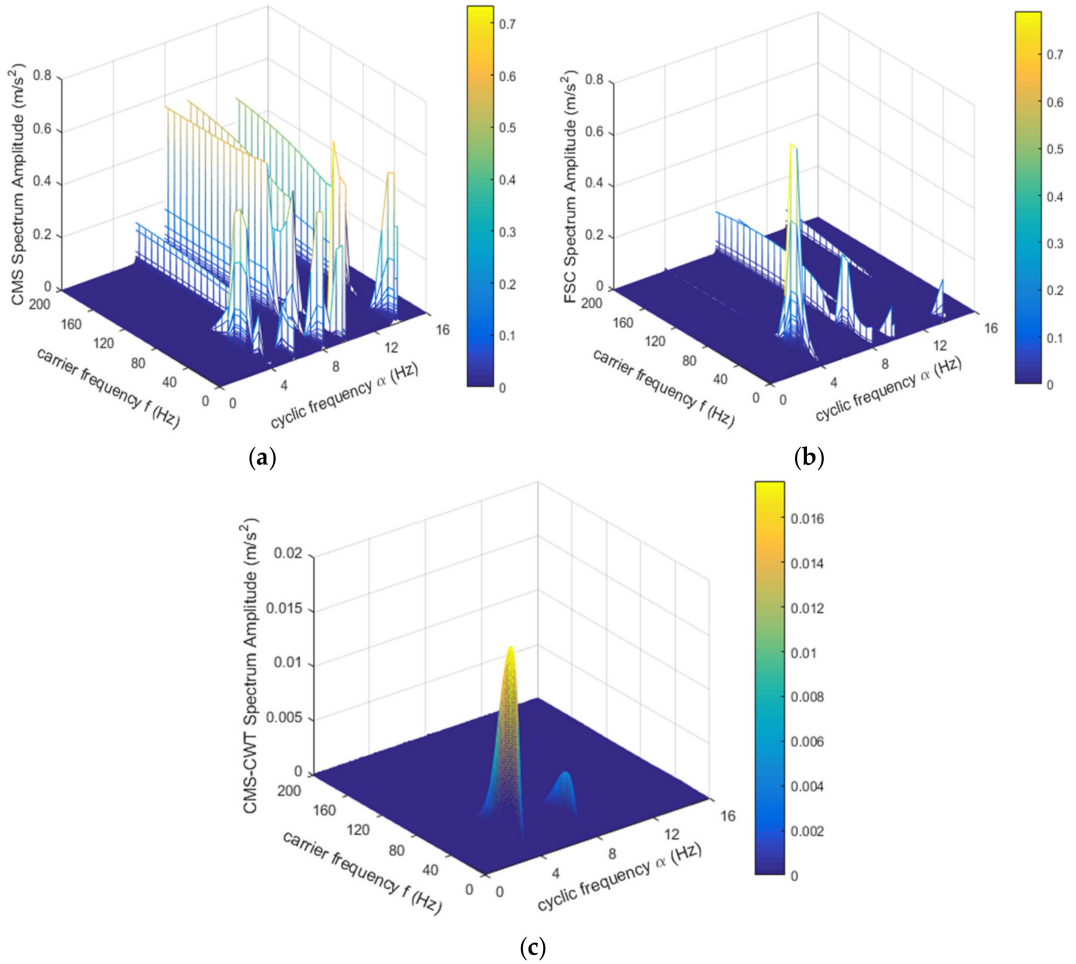

Figure 6. Three-dimensional vibration spectrum analysed by (**a**) CMS, (**b**) FSC, and (**c**) CMS-CWT with *Fs* = 1000 Hz.

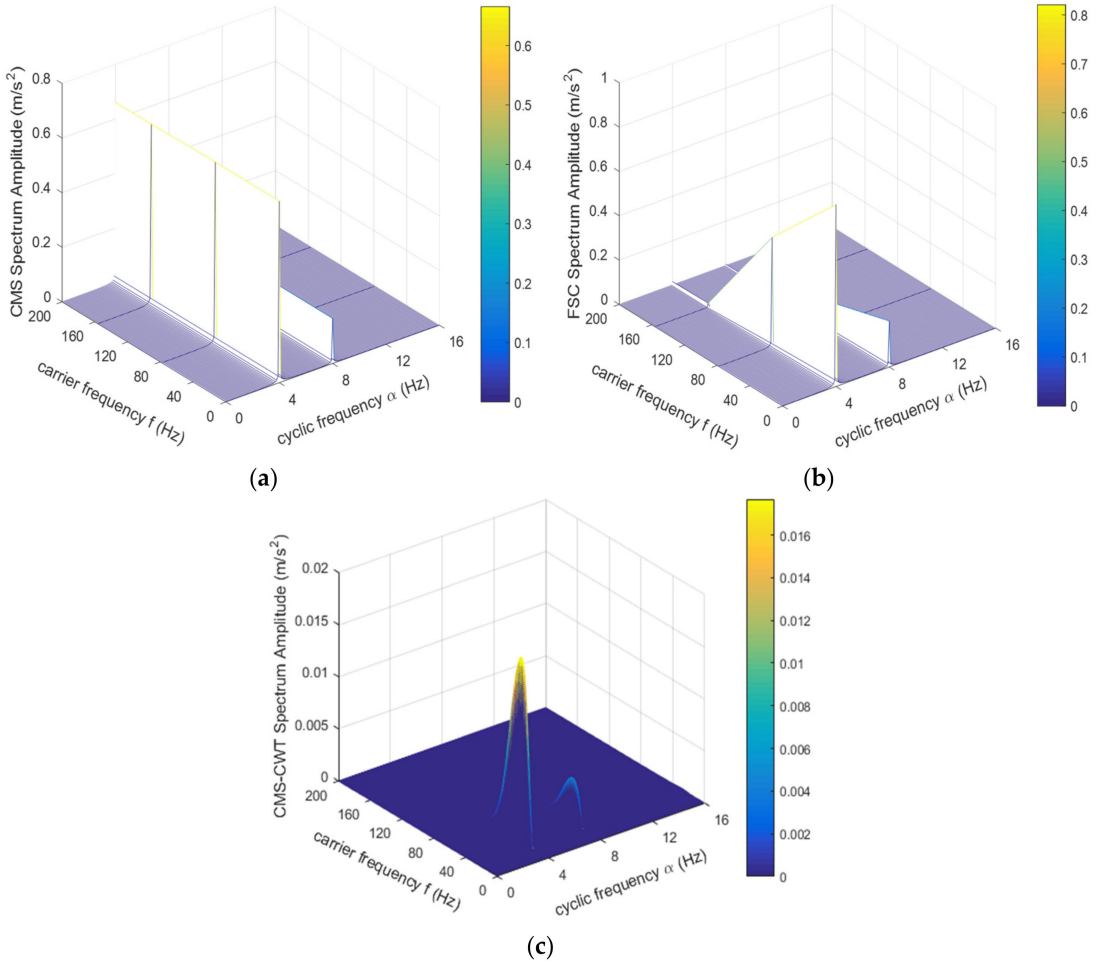

Figure 7. Three-dimensional vibration spectrum analysed by (**a**) CMS, (**b**) FSC, and (**c**) CMS-CWT with *Fs* = 10,000 Hz.

4. Experimental Validation and Discussion

4.1. Experimental Setup

In this section, the BRB fault data issued from IMs was utilized to evaluate the performance of the CMS-CWT algorithm. The IM test rig was used to collect the vibration signals from a faulty motor with 1 BRB fault and a baseline (health) motor. Figure 8 shows the test rig applied to the experimental study. Meanwhile, the motors were also tested under a series of load conditions to evaluate the load dependency of the proposed approach. The system consists of a drive motor, a coupling, a DC load generator, an encoder, a thermocouple, a horizontal accelerometer, and a vertical accelerometer. The tested motor is a 2-pole pairs IM with rated speed of 1500 rpm. As illustrated in Figure 9, the fault case is a motor with 1 BRB which was created by drilling a hole into one bar up to its full depth. Vibration signals of the testing motor were measured by a vertical and a horizontal accelerometer. The encoder mounted at the free end of the motor was utilized to measure motor speed and slip for the calculation of fault frequency.

To examine the performance of proposed method in detecting BRB faults, the vibration signals were measured under different operating conditions under 0%, 20%, 40% to 80% of the full operating load and at the rated frequency. All the measurements were sampled with a high-speed data acquisition system at a sampling rate of 96 kHz per channel. A data length of 20 s was acquired in order to achieve a good analysis in evaluating CMS-CWT method.

In addition, the Hamming window with the length of 2^8 and the step size of 35% of the window length (R = 89) was utilized for the signal processing. As a result, the maximum cycle frequency that could be analyzed by the CMS and the FSC was approximately 375 Hz and 539 Hz, respectively; thus the loop frequency analysis range was enough to support for the analysis of BRB faults.

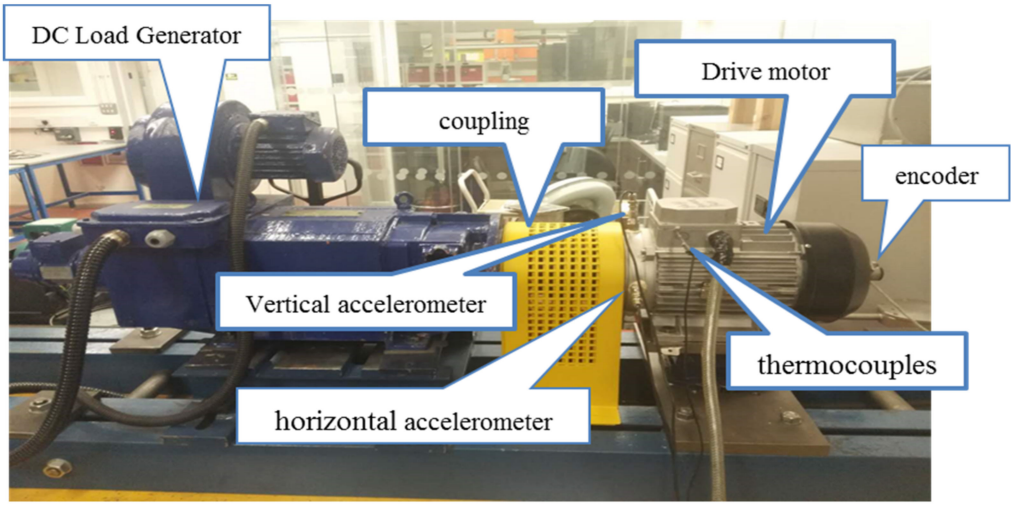

Figure 8. Experimental setup.

Figure 9. The faulty rotor simulated with one bar breakage.

4.2. Experimental Results and Discussion

It has been observed that the characteristic frequency 2 *sf* (where *s* is the slip and *f* is the supply frequency) is the most dominating fault component and easily obvious owing to its higher power in comparison to other fault frequency components corresponding to MVSA. When the BRB fault occurs, a torque ripple and a speed oscillation will be generated at frequency 2 *sf*, which is modulated on the rotation frequency components. Hence, this characteristic frequency will be extracted and analyzed using faulty motor with 1 BRB in the following experimental analysis for determining the robustness of proposed methodology.

As shown in Figure 10a,b, the STFT-based CMS and FSC yield approximate rough results, and they provide a long carrier frequency band modulated by the fault frequency. It was difficult to find the specific carrier frequency bandwidth modulated by fault frequency content. However, the CMS based on CWT presented a relatively accurate and narrow carrier frequency bandwidth modulated by fault frequency as shown in Figure 10c. Therefore, the spectrum obtained from CMS-CWT has the ability to clearly identify and present the approximate range of carrier frequency components modulated by the cyclic frequency related to BRB faults. The precise wavelet analysis can gather the energy of

information related to BRB faults, so that it can satisfy the requirement of cyclic frequency and carrier frequency location.

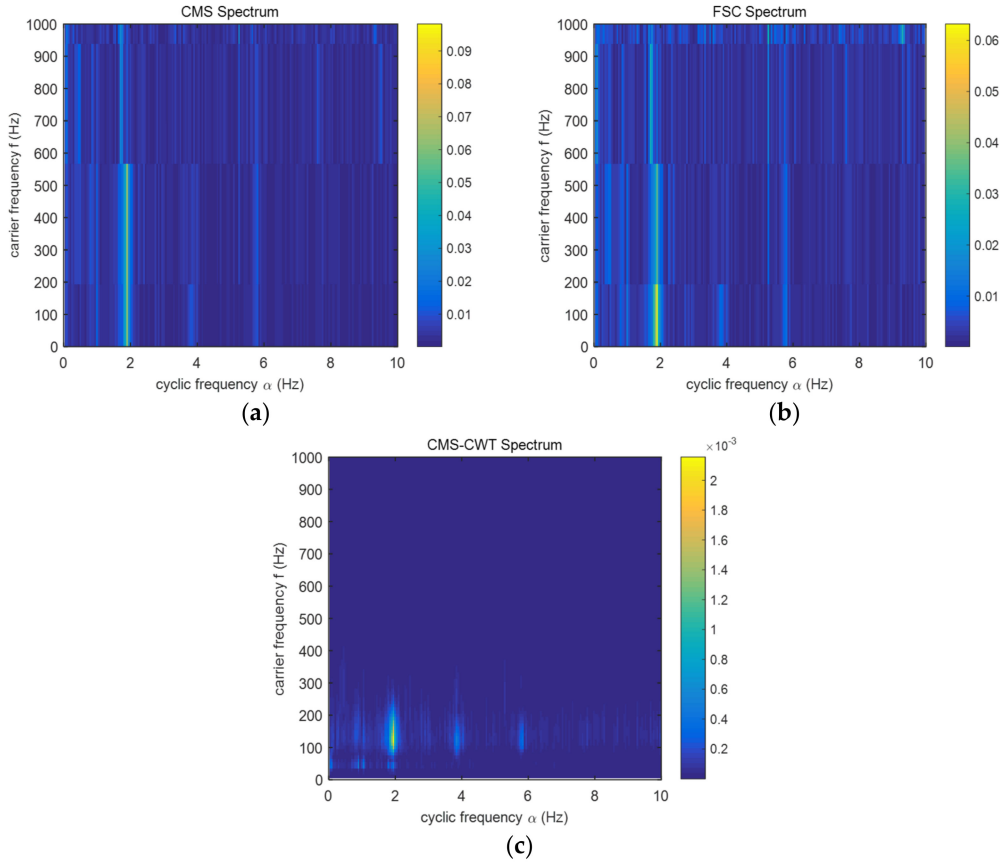

Figure 10. Carrier frequency identification capability of (**a**) CMS, (**b**) FSC, and (**c**) CMS-CWT for the one broken bar case under 40% load.

The slips of the IM with 1 BRB fault under different loads and their fault frequency components calculated by CMS, FSC, and CMS-CWT methods according to the characteristic frequency 2 *sf* were presented in Table 3. Based on the analysis results, all the three cyclostationary analysis methods can accurately extract fault modulation components because of higher cycle frequency resolution. Meanwhile, the fault frequency 2 *sf* is indeed effective to confirm the presence of BRB failure in IMs.

Table 3. The slips and characteristic frequencies under different loads.

Load	Slip (*s*)	Characteristic Frequency α = 2 *sf* (Hz)	CMS	FSC	CMS-CWT
	1 BRB		1 BRB	1 BRB	1 BRB
0%	0.002	0.20	0.20	0.20	0.20
20%	0.010	1.00	0.95	0.95	0.95
40%	0.018	1.80	1.75	1.75	1.75
80%	0.036	3.60	3.65	3.65	3.65

Diagnosis of BRB fault signature using CMS and FSC vibration spectrums under 0%, 20%, 40%, and 80% load conditions are shown in Figures 11 and 12. It can be seen that CMS and FSC based on STFT received similar results. In a comparison with the experimental results issued from CMS-CWT as shown in Figure 13, the analysis results obtained from CMS and FSC indeed present additional harmonic components with big amplitudes or interference components that affecting the extraction of main characteristic frequency 2 *sf*, especially under the low load states such as 0%, 20%, and 40%

load conditions. However, this unimportant interference components were not visible in CMS-CWT vibration spectrum as presented in Figure 13. On the one hand, it demonstrated that the CMS-CWT is able to get better detectability in diagnosing the presence of BRB fault from light loads to high loads. On the other hand, this method exhibited an excellent performance and a high sensitivity to BRB fault information because of its high frequency resolution. More importantly, the CMS-CWT further improved the detection precision.

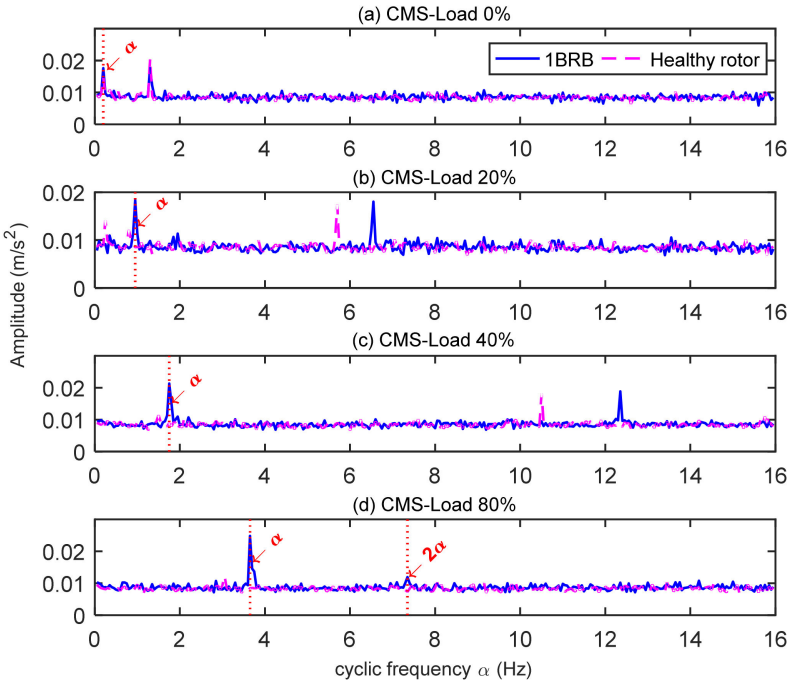

Figure 11. Vibration spectrum of the healthy induction motor and faulty motor with one broken rotor bar (BRB) analyzed by CMS under (**a**) 0% load, (**b**) 20% load, (**c**) 40% load, and (**d**) 80% load.

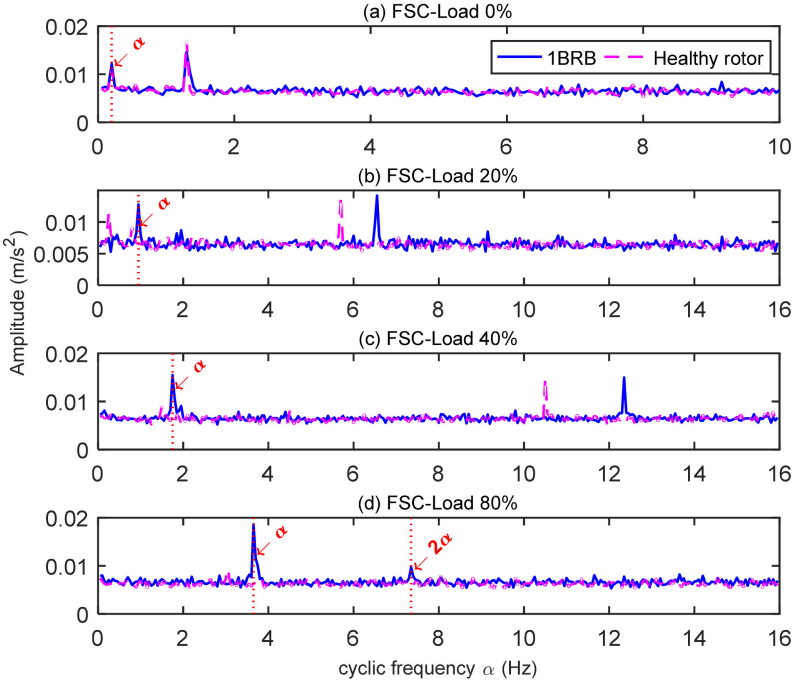

Figure 12. Vibration spectrum of the healthy induction motor and faulty motor with one BRB analysed by FSC under (**a**) 0% load, (**b**) 20% load, (**c**) 40% load, and (**d**) 80% load.

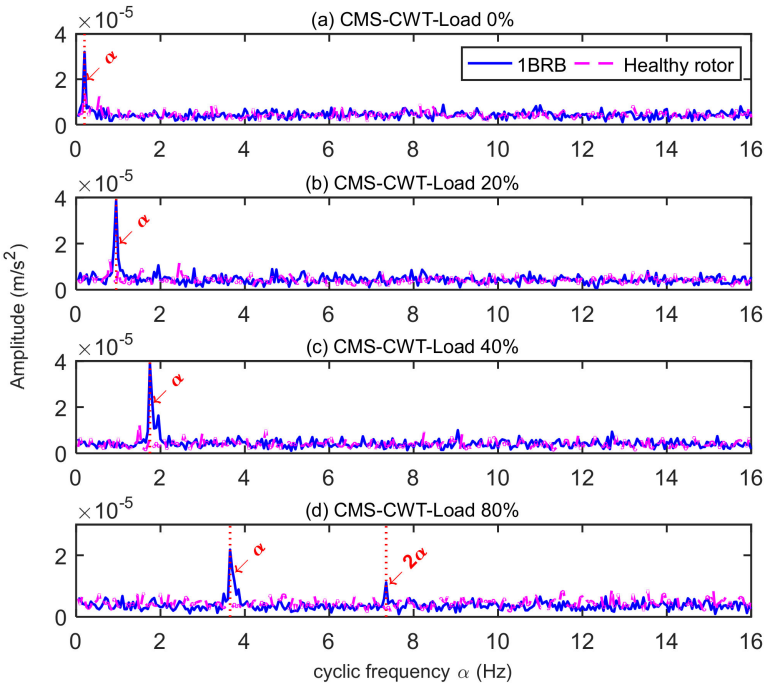

Figure 13. Vibration spectrum of the healthy induction motor and damaged motor with one BRB analyzed by CMS-CWT under (**a**) 0% load, (**b**) 20% load, (**c**) 40% load, and (**d**) 80% load.

5. Conclusions

The cyclostationary analysis indeed is an effective tool in the identification and extraction of mechanical faults caused by the modulation of low frequency components based on the cyclostationary level. However, the CMS and FSC based on the STFT have the limitations of low carrier frequency resolution and limited analysis range of cyclic frequency. Therefore, it is difficult to identify the carrier frequency information modulated by fault contents accurately, and it will produce the undesired harmonic components or non-faulty components under low loads effecting the extraction of characteristic frequency for the distinction of mechanical faults. This study proposed an improved CMS analysis method based on CWT which can achieve better demodulation results with higher carrier frequency resolution. Moreover, the proposed CMS-CWT approach can enhance the accuracy of fault identification regardless of whether it is in the cyclic frequency domain or in the carrier frequency domain, due to the fact that the CWT can automatically adjust the window size to achieve a comprehensive analysis of the signal to overcome the shortcomings of STFT. The simulation and experimental analysis results demonstrated the proposed method can achieve better performance than conventional CMS and FSC in reducing the possibility of unexpected downtime of the IMs. Finally, the proposed technique has the potential to be applied to detect other types of faults for rotating machinery fault diagnosis which presents better prospect in the practical applications.

Author Contributions: D.Z. and H.Z. investigated and designed the method, Z.W. and H.L. analyzed the data, J.Y. and F.G. were responsible for the subject revision. All the authors have read and approved the final manuscript.

Funding: This research was funded by the National Natural Science Foundation of China, grant number 51605133, 51705127 and the Hebei Province Science and Technology Support Program, China, grant number 17394303D.

Acknowledgments: The authors would like to thank Centre for Efficiency and Performance Engineering (CEPE) at the University of Huddersfield for providing the materials used for experiments. Meanwhile, the authors would like to appreciate anonymous reviewers and editors for their valuable comments and constructive suggestions.

Conflicts of Interest: The authors declare no conflict of interest.

References

1. Choudhary, A.; Goyal, D.; Shimi, S.L.; Akula, A. Condition monitoring and fault diagnosis of induction motors: A review. *Arch. Comput. Methods Eng.* **2018**, *25*, 1–18. [CrossRef]
2. Pineda-Sanchez, M.; Puche-Panadero, R.; Martinez-Roman, J.; Sapena-Bano, A.; Riera-Guasp, M.; Perez-Cruz, J. Partial Inductance Model of Induction Machines for Fault Diagnosis. *Sensors* **2018**, *18*, 2340. [CrossRef] [PubMed]
3. Burriel-Valencia, J.; Puche-Panadero, R.; Martinez-Roman, J.; Sapena-Bano, A.; Pineda-Sanchez, M. Fault Diagnosis of Induction Machines in a Transient Regime Using Current Sensors with an Optimized Slepian Window. *Sensors* **2018**, *18*, 146. [CrossRef] [PubMed]
4. Hernández, J.C.; Antonino-Daviu, J.; Martínez-Giménez, F.; Peris, A. Comparison of different wavelet families for broken bar detection in induction motors. In Proceedings of the 2015 IEEE International Conference on Industrial Technology (ICIT), Seville, Spain, 17–19 March 2015; pp. 3220–3225.
5. Lizarraga-Morales, R.A.; Rodriguez-Donate, C.; Cabal-Yepez, E.; Lopez-Ramirez, M.; Ledesma-Carrillo, L.M.; Ferrucho-Alvarez, E.R. Novel FPGA-based methodology for early broken rotor bar detection and classification through homogeneity estimation. *IEEE Trans. Instrum. Meas.* **2017**, *66*, 1760–1769. [CrossRef]
6. Abd-el-Malek, M.; Abdelsalam, A.K.; Hassan, O.E. Induction motor broken rotor bar fault location detection through envelope analysis of start-up current using Hilbert transform. *Mech. Syst. Signal Process.* **2017**, *93*, 332–350. [CrossRef]
7. Rangel-Magdaleno, J.; Peregrina-Barreto, H.; Ramirez-Cortes, J.; Morales-Caporal, R.; Cruz-Vega, I. Vibration Analysis of Partially Damaged Rotor Bar in Induction Motor under Different Load Condition Using DWT. *Shock. Vib.* **2016**, *2016*, 1–11. [CrossRef]
8. Gu, F.; Wang, T.; Alwodai, A.; Tian, X.; Shao, Y.; Ball, A.D. A new method of accurate broken rotor bar diagnosis based on modulation signal bispectrum analysis of motor current signals. *Mech. Syst. Signal Process.* **2015**, *50*, 400–413. [CrossRef]
9. Rangel-Magdaleno, J.; Peregrina-Barreto, H.; Ramirez-Cortes, J.; Cruz-Vega, I. Hilbert spectrum analysis of induction motors for the detection of incipient broken rotor bars. *Measurement* **2017**, *109*, 247–255. [CrossRef]
10. Zolfaghari, S.; Noor, S.B.M.; Mehrjou, M.R.; Marhaban, M.H.; Mariun, N. Broken Rotor Bar Fault Detection and Classification Using Wavelet Packet Signature Analysis Based on Fourier Transform and Multi-Layer Perceptron Neural Network. *Appl. Sci.* **2017**, *8*, 25. [CrossRef]
11. Bessam, B.; Menacer, A.; Boumehraz, M.; Cherif, H. DWT and Hilbert transform for broken rotor bar fault diagnosis in induction machine at low load. *Energy Procedia* **2015**, *74*, 1248–1257. [CrossRef]
12. Mustafa, M.O.; Nikolakopoulos, G.; Gustafsson, T.; Kominiak, D. A fault detection scheme based on minimum identified uncertainty bounds violation for broken rotor bars in induction motors. *Control Eng. Pract.* **2016**, *48*, 63–77. [CrossRef]
13. Shi, P.; Chen, Z.; Vagapov, Y.; Zouaoui, Z. A new diagnosis of broken rotor bar fault extent in three phase squirrel cage induction motor. *Mech. Syst. Signal Process.* **2014**, *42*, 388–403. [CrossRef]
14. Rivera-Guillen, J.R.; De Santiago-Perez, J.J.; Amezquita-Sanchez, J.P.; Valtierra-Rodriguez, M.; Romero-Troncoso, R.J. Enhanced FFT-based method for incipient broken rotor bar detection in induction motors during the startup transient. *Measurement* **2018**, *124*, 277–285. [CrossRef]
15. Quiroz, J.C.; Mariun, N.; Mehrjou, M.R.; Izadi, M.; Misron, N.; Radzi, M.A.M. Fault detection of broken rotor bar in LS-PMSM using random forests. *Measurement* **2018**, *116*, 273–280. [CrossRef]
16. Camarena-Martinez, D.; Perez-Ramirez, C.A.; Valtierra-Rodriguez, M.; Amezquita-Sanchez, J.P.; de Jesus Romero-Troncoso, R. Synchrosqueezing transform-based methodology for broken rotor bars detection in induction motors. *Measurement* **2016**, *90*, 519–525. [CrossRef]
17. Singh, G.; Naikan, V.N.A. Detection of half broken rotor bar fault in VFD driven induction motor drive using motor square current MUSIC analysis. *Mech. Syst. Signal Process.* **2018**, *110*, 333–348. [CrossRef]
18. Bellini, A.; Concari, C.; Franceschini, G.; Tassoni, C.; Toscani, A. Vibrations, currents and stray flux signals to asses induction motors rotor conditions. In Proceedings of the IECON 2006-32nd Annual Conference on IEEE Industrial Electronics, Paris, France, 6–10 November 2006; pp. 4963–4968.
19. De Jesus Rangel-Magdaleno, J.; de Jesus Romero-Troncoso, R.; Osornio-Rios, R.A.; Cabal-Yepez, E.; Contreras-Medina, L.M. Novel methodology for online half-broken-bar detection on induction motors. *IEEE Trans. Instrum. Meas.* **2009**, *58*, 1690–1698. [CrossRef]

20. Oviedo, S.J.; Quiroga, J.E.; Borras, C. Experimental evaluation of motor current signature and vibration analysis for rotor broken bars detection in an induction motor. In Proceedings of the 2011 International Conference on Power Engineering, Energy and Electrical Drives, Malaga, Spain, 11–13 May 2011; pp. 1–6.
21. Gritli, Y.; Di Tommaso, A.O.; Filippetti, F.; Miceli, R.; Rossi, C.; Chatti, A. Investigation of motor current signature and vibration analysis for diagnosing rotor broken bars in double cage induction motors. In Proceedings of the International Symposium on Power Electronics Power Electronics, Electrical Drives, Automation and Motion, Sorrento, Italy, 20–22 June 2012; pp. 1360–1365.
22. Gritli, Y.; Di Tommaso, A.O.; Miceli, R.; Filippetti, F.; Rossi, C. Vibration signature analysis for rotor broken bar diagnosis in double cage induction motor drives. In Proceedings of the 4th International Conference on Power Engineering, Energy and Electrical Drives, Istanbul, Turkey, 13–17 May 2011; pp. 1814–1820.
23. Kanović, Ž.; Matić, D.; Jeličić, Z.; Rapaić, M.; Jakovljević, B.; Kapetina, M. Induction motor broken rotor bar detection using vibration analysis—A case study. In Proceedings of the 2013 9th IEEE International Symposium on Diagnostics for Electric Machines, Power Electronics and Drives (SDEMPED), Valencia, Spain, 27–30 August 2013; pp. 64–68.
24. Miceli, R.; Gritli, Y.; Di Tommaso, A.; Filippetti, F.; Rossi, C. Vibration signature analysis for monitoring rotor broken bar in double squirrel cage induction motors based on wavelet analysis. *COMPEL Int. J. Comput. Math. Electr. Electron. Eng.* **2014**, *33*, 1625–1641. [CrossRef]
25. Kumar, T.C.A.; Singh, G.; Naikan, V.N.A. Effectiveness of vibration and current monitoring in detecting broken rotor bar and bearing faults in an induction motor. In Proceedings of the 2016 IEEE 6th International Conference on Power Systems (ICPS), New Delhi, India, 4–6 March 2016; pp. 1–5.
26. Vincent, J.; Tamilselvan, A. Vibration analysis of 3-phase squirrel cage induction motor due to broken rotor using artificial intelligence. In Proceedings of the 2016 International Conference on Emerging Trends in Engineering, Technology and Science (ICETETS), Pudukkottai, India, 24–26 February 2016; pp. 1–4.
27. Morales-Perez, C.; Rangel-Magdaleno, J.; Peregrina-Barreto, H.; Ramirez-Cortes, J. Half-broken rotor bar detection on im by using sparse representation under different load conditions. In Proceedings of the 2017 IEEE International Autumn Meeting on Power, Electronics and Computing (ROPEC), Ixtapa, Mexico, 8–10 November 2017; pp. 1–5.
28. Martinez, J.; Belahcen, A.; Muetze, A. Analysis of the vibration magnitude of an induction motor with different numbers of broken bars. *IEEE Trans. Ind. Appl.* **2017**, *53*, 2711–2720. [CrossRef]
29. Morales-Perez, C.; Rangel-Magdaleno, J.; Peregrina-Barreto, H.; Amezquita-Sanchez, J.P.; Valtierra-Rodriguez, M. Incipient broken rotor bar detection in induction motors using vibration signals and the orthogonal matching pursuit algorithm. *IEEE Trans. Instrum. Meas.* **2018**, *67*, 2058–2068. [CrossRef]
30. Xie, Y.; Chen, P.; Li, F.; Liu, H. Electromagnetic forces signature and vibration characteristic for diagnosis broken bars in squirrel cage induction motors. *Mech. Syst. Signal Process.* **2019**, *123*, 554–572. [CrossRef]
31. Delgado-Arredondo, P.A.; Morinigo-Sotelo, D.; Osornio-Rios, R.A.; Avina-Cervantes, J.G.; Rostro-Gonzalez, H.; de Jesus Romero-Troncoso, R. Methodology for fault detection in induction motors via sound and vibration signals. *Mech. Syst. Signal Process.* **2017**, *83*, 568–589. [CrossRef]
32. Lee, J.H.; Pack, J.H.; Lee, I.S. Fault Diagnosis of Induction Motor Using Convolutional Neural Network. *Appl. Sci.* **2019**, *9*, 2950. [CrossRef]
33. Picazo-Rodenas, M.J.; Antonino-Daviu, J.; Climente-Alarcon, V.; Royo-Pastor, R.; Mota-Villar, A. Combination of noninvasive approaches for general assessment of induction motors. *IEEE Trans. Ind. Appl.* **2014**, *51*, 2172–2180. [CrossRef]
34. Ceban, A.; Pusca, R.; Romary, R. Study of rotor faults in induction motors using external magnetic field analysis. *IEEE Trans. Ind. Electron.* **2011**, *59*, 2082–2093. [CrossRef]
35. Hao, Y.; Song, L.; Wang, M.; Cui, L.; Wang, H. Underdetermined source separation of bearing faults based on optimized intrinsic characteristic-scale decomposition and local non-negative matrix factorization. *IEEE Access* **2019**, *7*, 11427–11435. [CrossRef]
36. Wan, S.; Li, H.M.; Li, Y.G. Analysis on vibration characteristics of generator with the fault of eccentric air-gap. *J. Vib. Shock* **2005**, *24*, 21–23.
37. Wan, S.T.; Li, H.M.; Xu, Z.F.; Li, Y.G. Analysis of generator vibration characteristic on stator winding inter-turn short circuit fault. *Proc. CSEE* **2004**, *4*, 20.
38. Antoni, J. Cyclostationarity by examples. *Mech. Syst. Signal Process.* **2009**, *23*, 987–1036. [CrossRef]

39. Borghesani, P. The envelope-based cyclic periodogram. *Mech. Syst. Signal Process.* **2015**, *58*, 245–270. [CrossRef]
40. Antoni, J. Cyclic spectral analysis in practice. *Mech. Syst. Signal Process.* **2007**, *21*, 597–630. [CrossRef]
41. Antoni, J.; Xin, G.; Hamzaoui, N. Fast computation of the spectral correlation. *Mech. Syst. Signal Process.* **2017**, *92*, 248–277. [CrossRef]
42. Ni, S.H.; Yang, Y.Z.; Tsai, P.H.; Chou, W.H. Evaluation of pile defects using complex continuous wavelet transform analysis. *NDT E Int.* **2017**, *87*, 50–59. [CrossRef]
43. Wang, H.; Ren, B.; Song, L.; Cui, L. A novel weighted sparse representation classification strategy based on dictionary learning for rotating machinery. *IEEE Trans. Instrum. Meas.* **2019**. [CrossRef]
44. Yang, Y.; Peng, Z.; Zhang, W.; Meng, G. Parameterised time-frequency analysis methods and their engineering applications: A review of recent advances. *Mech. Syst. Signal Process.* **2019**, *119*, 182–221. [CrossRef]
45. Xia, C.; Liu, C. Identification and Representation of Multi-Pulse Near-Fault Strong Ground Motion Using Adaptive Wavelet Transform. *Appl. Sci.* **2019**, *9*, 259. [CrossRef]